RESEARCH ARTICLE
doi: 10.2306/scienceasia1513-1874.2024.066

ScienceAsia 50 (3): 2024: ID 2024066: **1–9**

Preparation of calcium oxide/graphitic carbon nitrides (CaO/g-C_3N_4) composite for photocatalyst dye degradation

Chinanun Chaisrisongkram, Thutiyaporn Thiwawong, Korakot Onlaor, Benchapol Tunhoo*

Electronics and Control System for Nanodevice Research Laboratory, College of Materials Innovation and Technology, King Mongkut's Institute of Technology Ladkrabang, Bangkok 10520 Thailand

*Corresponding author, e-mail: benchapol.tu@kmitl.ac.th

Received 22 Jun 2023, Accepted 12 Jun 2024
Available online 21 Jul 2024

ABSTRACT: Dye degradation properties of composited calcium oxide (CaO) and graphitic carbon nitride (g-C_3N_4) were studied. The CaO and g-C_3N_4 nanoparticles were derived under separate thermal calcination processes from eggshells and melamine, respectively. Physical properties of the synthesized CaO and g-C_3N_4 were investigated by X-ray diffractometry (XRD), Fourier-transform infrared spectroscopy (FTIR), and scanning electron microscopy (SEM). The synthesized CaO and g-C_3N_4 nanoparticles were, then, composited at various concentrations, and the photocatalytic behaviors of the composited samples were investigated in an aqueous solution of methylene blue, with a irradiation source of 220 W white light-emitting diode lamp. Results showed that the optimal ratio of the composite material for dye degradation was 10% CaO:90% g-C_3N_4, giving 95.89% degradation efficiency with an exposure time of 15 min and degradation rate of 0.1727 min^{-1}.

KEYWORDS: calcium oxide, dye degradation, graphitic carbon nitride, composite material

INTRODUCTION

During photocatalysis, organic and inorganic contaminants in water or air are removed from the surface of the catalyst material. Typically, the process is achieved in an aqueous phase called photooxidation [1]. Charge carriers, such as electrons and holes, can transfer electric charges between acceptor and donor levels in solutions. Therefore, photon energy from the irradiated light source plays an important role in photocatalysis. Various light wavelengths can be used for photocatalyst application, such as ultraviolet, visible light, and infrared [2].

Composite materials have unique properties and are used in many applications, including electronic device, health, food, environment and photocatalysis. Materials such as ZnO, TiO_2, and graphitic carbon nitride (g-C_3N_4) have been used for photo-induced catalysis of chemical transformations to degrade dye solutions [3]. When a composite is used as catalyst for photocatalytic activity, the photon energy of irradiated light is related to the energy band gap of the material; and the excited charges can be transferred between the donor and the acceptor states, which is the electron-hole separation [4]. Charges transferred between states are involved in chemical reactions such as oxidation or reduction. Photogenerated charges react with contaminants from degradation, water splitting, and disinfection [5].The charge carriers can easily recombine, and the process of charge transfer is influenced by the material's or device's structures, e.g. heterojunction or composite. The structures impact the mechanisms, characteristics, and performances of photocatalytic behavioral properties [6].

Chicken eggs are a common food in human households, with eggshells as the only waste. Eggshells are mainly composed of calcium carbonate ($CaCO_3$) [7]. Calcium from eggshells can be used for many applications, for example, in cosmetic industry and as a feed ingredient in livestock industry. Eggshells are used as a calcium source for calcium oxide (CaO) production, called calcination process. By sintering eggshells at high temperatures, $CaCO_3$ in the eggshells decomposes to CaO [8] and carbon dioxide (CO_2).

Melamine is a type of plastic that contains formaldehyde [8, 9], and is mainly used to make components, dishes, bags, wraps, cleaning agents, and fertilizers. Melamine has also been developed as a starter material for synthesizing graphitic carbon nitride (g-C_3N_4). Melamine has a relatively high nitrogen content of 66.6% by mass [10]. When melamine is heated to above 390 °C, its structural form starts to change. When the temperature increases from 550 to 600 °C, the melamine structural form changes to graphitic carbon nitride (g-C_3N_4). This group of carbon nitride compounds has a general structure of C_3N_4, composing of two main components: heptazine and poly (triazine imide) units depending on reaction conditions. The polymerization of cyanamide to dicyandiamide achieves varying degrees of condensation properties and g-C_3N_4 reactions [11]. The g-C_3N_4 has been used in photocatalyst applications with advantageous properties such as low-cost, non-toxic material, and the strong reduction ability of its photogenerated electrons [12–14]. However, the drawbacks of g-C_3N_4 in photocatalyst applications are easy charge carrier recombination, low absorption coefficient, and low

specific surface area [15]. Photocatalytic behavior of g-C_3N_4 can be improved by compositing it with other materials. The heterojunction systems of composite materials enhance photodegradation properties, with capabilities of oxidation and reduction. The g-C_3N_4 can be composited easily with other metal oxides such as ZnO [16], Bi_2WO_6 [17], etc. CaO is also a good candidate for photocatalyst material with high photocatalytic versatility. Physical properties of CaO, such as crystallite size and specific surface area, are substantial factors in photocatalyst applications. As aforementioned, CaO can be synthesized from waste eggshells, and it can be prepared on a large scale with low cost for practical production [18].

In this study, dye degradation materials were fabricated by synthesizing CaO and g-C_3N_4 nanosheet from waste chicken eggshells and thermal calcination of melamine, respectively. Physical properties of the synthetic particles were characterized, and dye-degrading behaviors of the composite material was studied by light irradiation to enable photocatalysis. The amounts of dye in the dye solution before and after irradiation were examined to determine the dye line digestibility of the fabricated dye degradation composites.

MATERIALS AND METHODS

Material preparation and characterization

Preparation and characterization of CaO and g-C_3N_4

The thermal calcination process was applied to prepare nanoparticle materials. For CaO nanoparticles, dried waste eggshells (from a local market in Bangkok, Thailand) were ground in a mortar for 30 min and then calcined at 1000 °C for 3 h. For g-C_3N_4 nanoparticles, melamine powder ($C_3H_6N_6$, Sigma-Aldrich, St. Louis, Missouri, USA) was sintered at 600 °C, followed by 520 °C for 2 h to achieve nanosheets of g-C_3N_4. Physical properties of the synthesized materials were characterized by an X-ray diffractometer (XRD, SmartLab, Rigaku, Japan), a Fourier-transform infrared spectrophotometer (FTIR, Spectrum Two, PerkinElmer), X-ray photoelectron spectroscopy (XPS, Axis Ultra DLD, Kratos, United Kingdom), transmission electron microscope (TEM, JEM-2100, JEOL, Japan), and an environment scanning electron microscope (E-SEM, HITACHI S-3400N, Japan).

Preparation of CaO/g-C_3N_4 composites and photocatalytic process

A metal mesh (3×1.5 cm^2) was used as the substrate of the photocatalyst layer. Before using, the mesh was cleaned in a sonication bath, followed by rinsing with deionized water, ethanol, and acetone; then drying with hot air. CaO/g-C_3N_4 composites were prepared by mixing synthesized CaO and g-C_3N_4 particles at various concentrations by weight in a solution of 1.5 g PMMA polymer ($[(CH_2C(CH_3)(CO_2CH_3)]_n$, Mw 120000, Sigma Aldrich) in 10 ml acetone. The PMMA acted as a binder and adhesive material for the prepared composites on the metal mesh substrate. The CaO and g-C_3N_4 solutions were coated on the substrates by a dip coating process to obtained the CaO/g-C_3N_4 composite films. The prepared films were left air-dried under ambient conditions and, then, kept in a dark chamber before testing in the photocatalyst process.

Methylene blue (MB) ($C_{16}H_{18}N_3ClS \cdot 3\,H_2O$, Carlo Erba, Val de Reuil, France) in an aqueous solution was used to investigate the photocatalytic behaviors of the prepared CaO/g-C_3N_4 composite film samples. The volume and the concentration of aqueous MB solution were kept at 3 ml and 8.75×10^{-6} M, respectively. The photocatalyst light source was a 220 W white light LED lamp with the irradiaCountrytion times varied between 0 and 15 min. The spectra of an LED lamp were obtained with a spectrophotometer (Avantes, AvaSpec-2048, Netherlands) and shown in Fig. S1. The spectra peak is approximated at 22471 cm^{-1} or 445 nm. The dye decomposition materials were then removed, and the aqueous solution was used to investigate the dye decomposition characteristics through absorption spectroscopy (T92+ Spectrophotometer, PG Instruments, United Kingdom). Dye decomposition parameters, degradation rate and efficiency, were record.

RESULTS AND DISCUSSION

Fig. 1(a) depicts the XRD spectra of synthesized CaO and g-C_3N_4 nanoparticles (NPs). The XRD pattern of CaO synthesized from waste eggshells calcined at 1000 °C demonstrated dominant diffraction peaks at 2θ angle were 32.28°, 37.45°, 53.87°, 64.39°, and 67.48°. The peaks were identified (following JCPFS No. 82-1691) as (111), (200), (220), (311), and (222) planes of CaO, respectively [19], indicating the dominant phases of CaO material [20]. The XRD spectra of eggshells calcinated at various temperatures were shown in Fig. S2. The optimal calcination temperature to obtain CaO nanoparticles was 1000 °C, with subtle XRD peaks of $Ca(OH)_2$ found at 2θ angle were 18.85°, 28.65°, 34.27°, 47.16°, and 50.97° [21]. The $Ca(OH_2)$ as well as $CaCO_3$ was another phase of CaO affected by photocatalytic activity [22]. In this study, all samples of CaO particles were prepared by thermal calcination at 1000 °C, and the influence of impurities phase of CaO similarly affected all samples. The g-C_3N_4 nanosheet diffraction pattern exhibited a dominant peak at 2θ angle of 27.94°, identified as the (002) plane of g-C_3N_4 [11]. Usually, bulk g-C_3N_4 is composed of stacking flake-like structures [23]. Thermal exfoliation during the transformation process of the bulk to g-C_3N_4 nanosheets slightly changed the in-plane structural packing motif, as shown by the XRD pattern [24]. The XRD spectra of the bulk and the nanosheets of g-C_3N_4 were shown in Fig. S3, confirming the formation of g-C_3N_4 nanosheets.

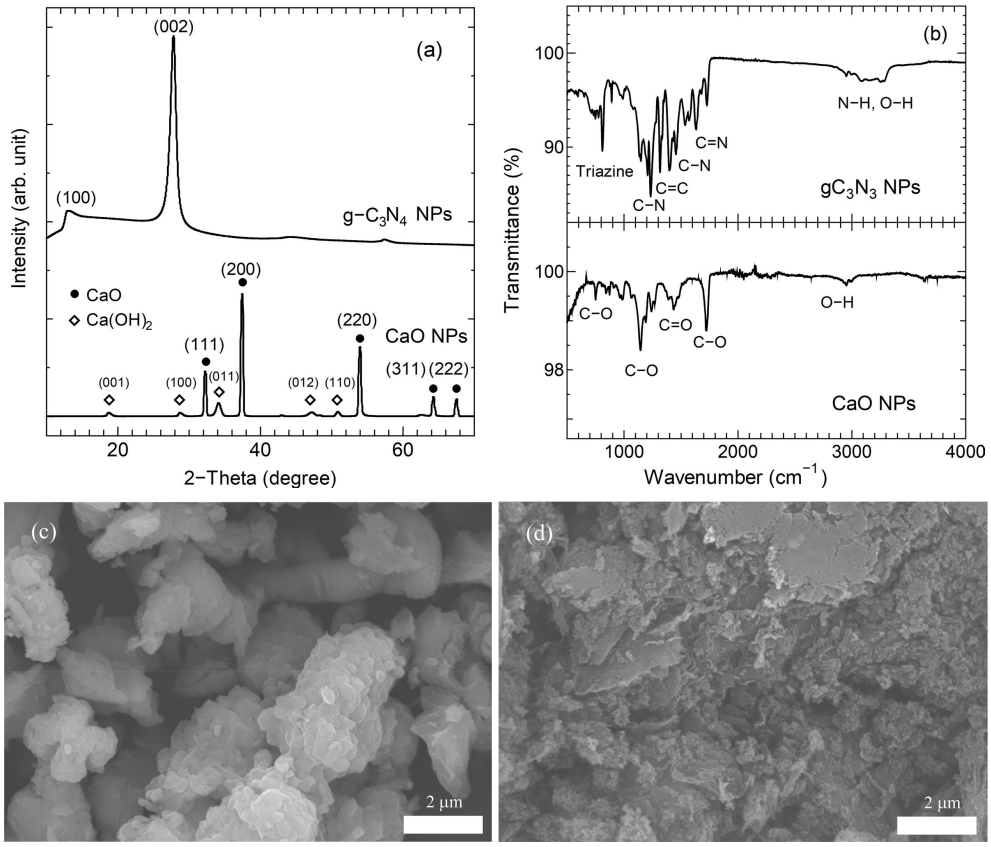

Fig. 1 (a), XRD patterns; (b) FTIR spectra; and (c)–(d), surface morphologies of CaO and g-C_3N_4 nanoparticles.

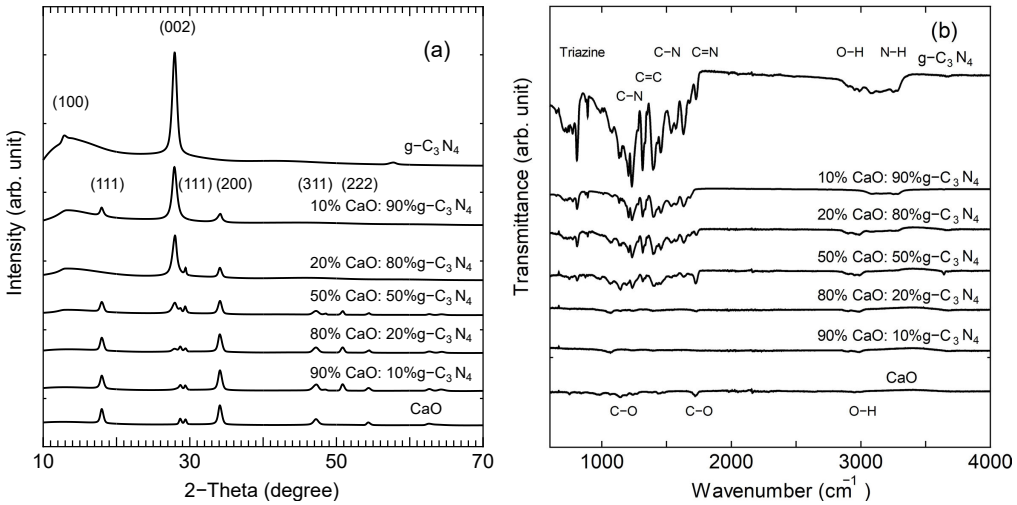

Fig. 2 (a), XRD patterns; and (b), FTIR spectra of CaO/g-C_3N_4 composite materials prepared with various ratios of CaO:g-C_3N_4 compared with Cao and g-C_3N_4.

Fig. 1(b) depicts the FTIR spectra of the CaO and the g-C_3N_4 nanoparticles. CaO showed dominant peaks at wavenumbers about 2947, 1719, 1444, 1145, and 752 cm^{-1}, correspondingly identified to functional groups of O—H, C—O, C=O, C—O, and C—O, respectively. For g-C_3N_4, the FTIR spectra showed

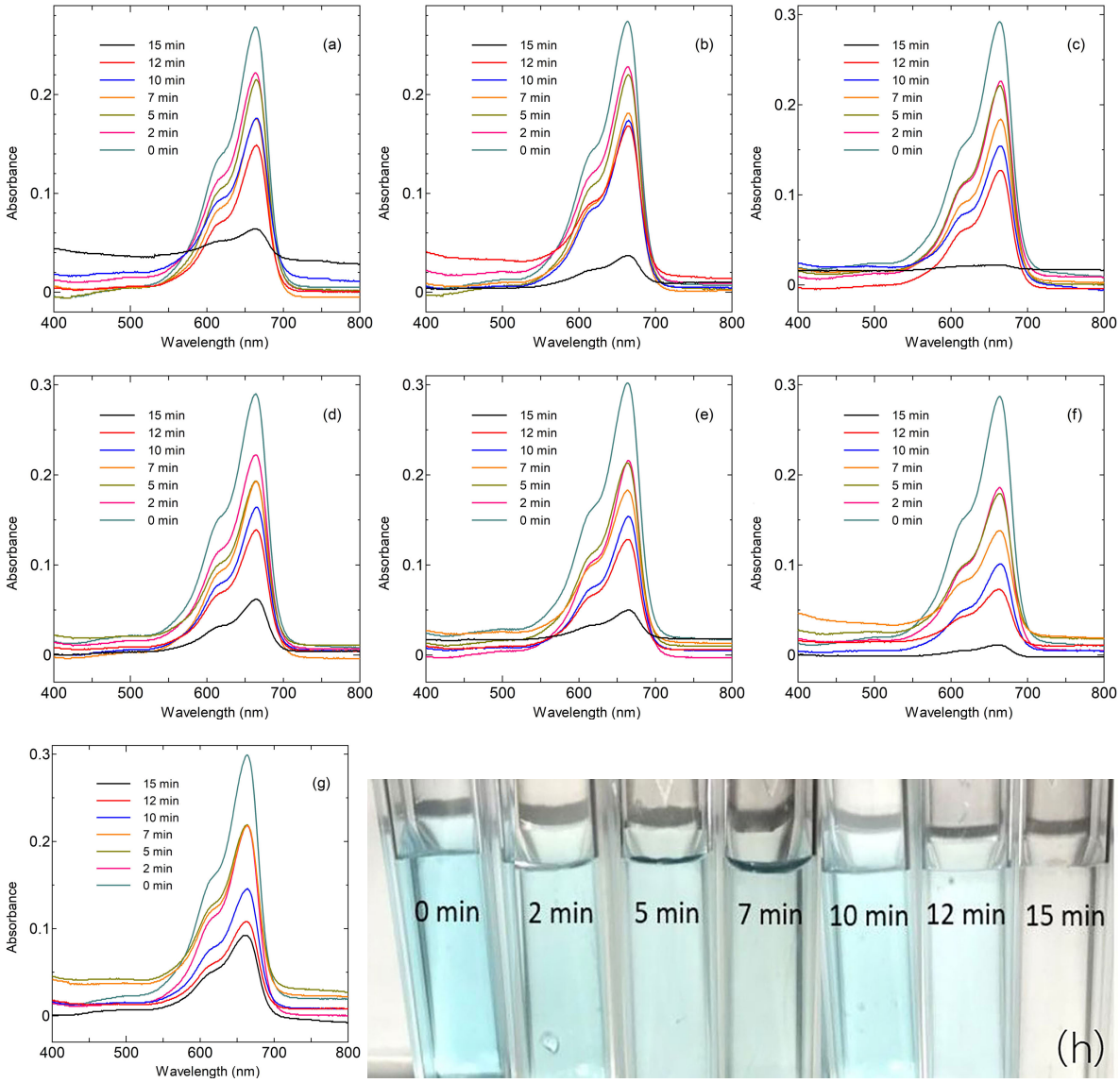

Fig. 3 Comparative photocatalytic activities of CaO/g-C_3N_4 composites prepared with different ratios (% wt.) of CaO:g-C_3N_4 at: (a), 100:0; (b), 90:10; (c), 80:20; (d), 50:50; (e), 20:80; (f), 10:90; (g), 0:100; and (h), image of aqueous MB solution photocatalyzed by 10% CaO:90% g-C_3N_4 composite for various irradiation times.

Table 1 Comparison of photocatalyst materials.

Photocatalyst material	Synthesis method	Light source	Dye solution	Degradation (%)	Irradiation time (min)	Ref.
Ag-Cu_2O/C_3N_4	Two steps reduction	500 W Xe lamp	MO	95.67	30	[38]
g-C_3N_4@Ag@$AgPO_4$	Etching	405 nm laser	RhB	94.80	60	[39]
Sn-WO_3/g-C_3N_4	Calcination	150 W halogen lamp	MO, RhB	87, 99	120, 50	[40]
WO_3/g-C_3N_4	Ultrasonication	300 W Xe lamp	MB	95	90	[41]
PAN/g-C_3N_4	Template free method	30 W LED lamp	MB	97.30	420	[42]
10% CaO:90% g-C_3N_4	Calcination	220 W LED lamp	MB	95.89	15	This study

MO, methylene orange; MB, methylene blue; RhB, rhodamine B.

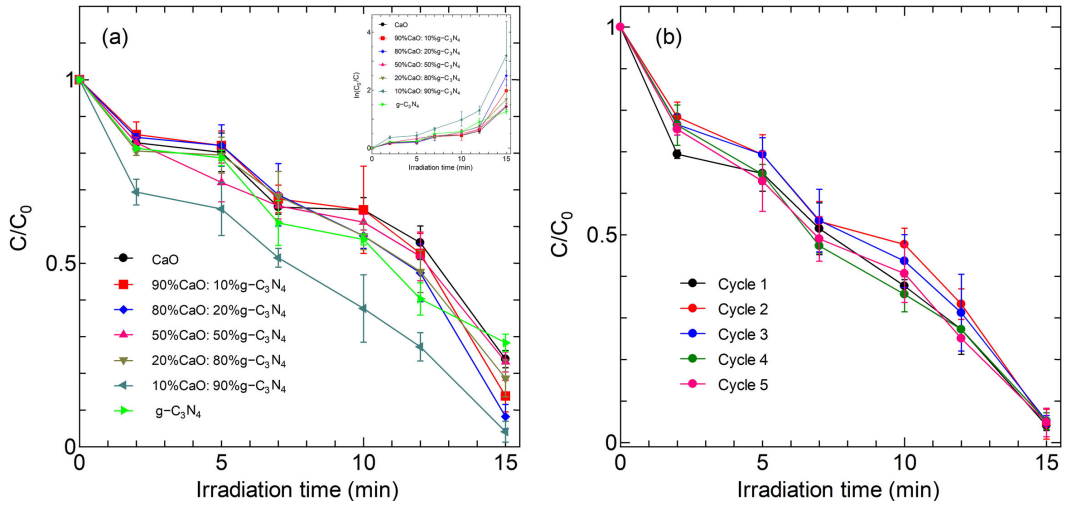

Fig. 4 (a), Comparison of C/C_0 values of CaO/g-C_3N_4 composites of different of CaO:g-C_3N_4 ratios and irradiation times (inset: C_0/C values in a logarithm scale versus irradiation time); and (b), photocatalyst cycling behaviors of 10% CaO:90% g-C_3N_4 composite on dye degradation.

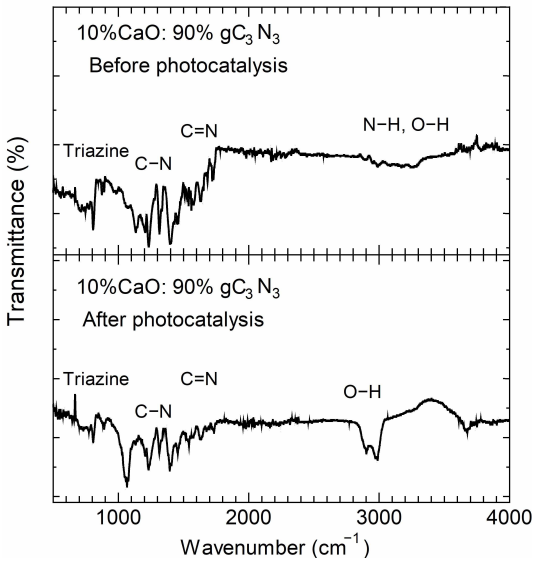

Fig. 5 FTIR spectra of 10% CaO:90% g-C_3N_4 for dye degradation before and after photocatalysis.

firm peaks at wavenumbers 1627, 1400, 1316, 1232, and 809 cm^{-1}, which were defined as C=N, C–N, C=C, C–N, and N–H functional groups (Triazine), respectively [25, 26]. The N–H and O–H stretching were identified at broad peaks 3070–3320 cm^{-1} [27]. The FTIR spectra were composed of native spectra and defect peaks due to the influence of preparation conditions.

Surface morphologies of the CaO and the g-C_3N_4 nanoparticles were shown in Fig. 1(c,d). Both CaO and g-C_3N_4 exhibited a particle-like structure. The CaO nanoparticles were spherical-like and clustered, while the g-C_3N_4 particles had layered structure clusters of polygon particles.

The XRD spectra of CaO/g-C_3N_4 composites prepared with various ratios by weight of CaO:g-C_3N_4 at 100%:0, 90%:10%, 80%:20%, 50%:50%, 20%:80%, 10%:90%, and 0:100% were shown in Fig. 2(a). The composite materials showed firm peaks at 2θ angles of 18.04°, 28.76°, 29.40°, 34.10°, 47.08°, and 50.78°; while peaks of CaO were identified as (111), (111), (200), (311), and (222) planes. The dominant phase of the composite was CaO mixed with peaks of g-C_3N_4, indicating a firm peak at 2θ angle of 27.94° and defined as the (002) plane of g-C_3N_4. Higher ratios of g-C_3N_4 demonstrated more substantial peaks of g-C_3N_4 and slight peaks of CaO in the composite materials [11, 20]. Separation of the CaO and the g-C_3N_4 phases was observed in the mixed composited materials. The X-ray photoelectron spectroscopy (XPS) and transmission electron microscope (TEM) results confirmed the formation of composite material of CaO and g-C_3N_4, as shown in Figs. S4 and S5

The XPS peaks can be used to provide information about the chemical states of elements. Fig. S4(a) shows the XPS spectra of Ca 2p of CaO and composite materials. The XPS peaks at 348.4 eV and 351.9 eV were observed to correlate with the binding energy of $2p_{3/2}$ and $2p_{1/2}$ of CaO. The binding energy of CaO/g-C_3N_4 composite exhibited similar patterns as pristine CaO particles while having lower intensity due to the influence of lower CaO contents in composite materials. Fig. S4(b) depicts the XPS spectra of O 1s energy level. The O 1s level of CaO showed three

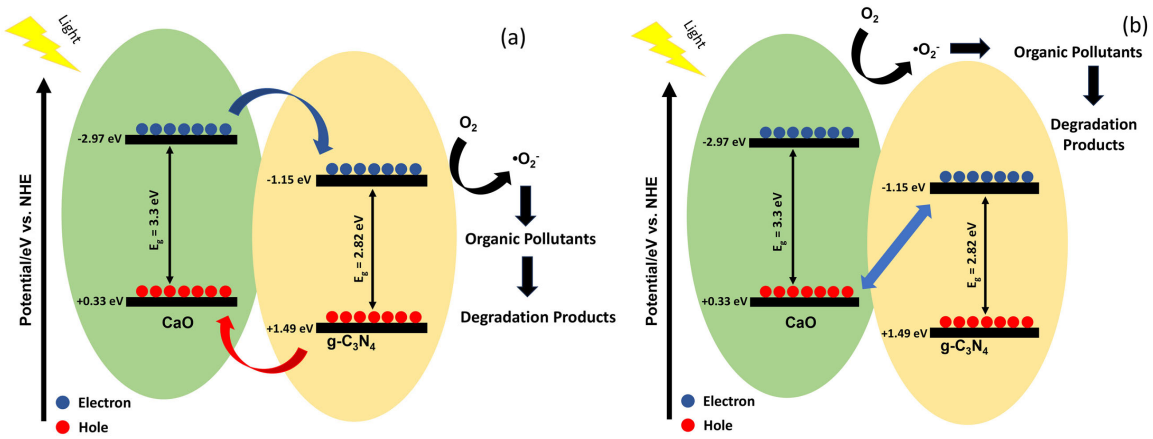

Fig. 6 Proposed mechanisms of dye photodegradation: (a), type-II photocatalyst; and (b), z-scheme photocatalyst.

components of 530.7 eV, 531.4 eV, and 532.3 eV, which corresponded to the lattice O_2, the absorbed O_2, and the O_2 of absorbed carbonates or water of CaO. For the g-C_3N_4, the three components of XPS spectra could be indicated as the carbonyl group (C=O), carboxy group (O=C–O), and the absorbed O_2 on the surface at the XPS peaks of 531.1 eV, 532.6 eV, and 534.0 eV [8]. The O 1s XPS peak component in the composite material was still observed with the carboxy group (O=C–O) at 532.3 eV. The N 1s binding energy spectra were shown in Fig. S4(c). The XPS peaks at 398.6 eV, 399.4 eV, 400.4 eV, and 401.3 eV could be due to sp^2-hybridized aromatic N atom of N–C=N, N atoms bound to tertiary carbon, amino functional groups of C–N–H, and tertiary nitrogen group (N–(C)3) of g-C_3N_4 [8, 9]. The N 1s XPS spectra of CaO/g-C_3N_4 composites demonstrated similarly with pristine g-C_3N_4.

In addition, Fig. S5(a) shows TEM images of CaO, which were well-defined crystalline particles with a regular shape and size. Fig. S5(b) shows a TEM image of g-C_3N_4 nanosheets with a layered structure and a clearly defined plane of atoms arranged in a hexagonal pattern. The layers appeared slightly curved, which is characteristic of the g-C_3N_4. The TEM picture of 10% wt. CaO:90% wt. g-C_3N_4 composite was shown in Fig. S5(c), demonstrating a composite structure of small CaO particles embedded in a g-C_3N_4 matrix.

The FTIR patterns of CaO/g-C_3N_4 composite materials were shown in Fig. 2(b). The FTIR peaks exhibited mixed characteristic peaks of CaO and g-C_3N_4. The peaks at wavenumbers 2947, 1719, 1145, and 752 cm^{-1} were identified as O–H, C–O, C–O, and C–O functional groups [10, 20], while peaks located at wavenumbers 3321, 3074, 1627, 1400, 1316, 1232, and 809 cm^{-1}, were identified as N–H group, O–H group, C=N group, C–N group, and triazine units of g-C_3N_4. The peak intensities depended on the weight compositions of the composite materials between CaO and g-C_3N_4, which represented the separation phase of the composite materials [25], corresponding to the XRD results.

The prepared CaO/g-C_3N_4 composites were used to assess their photocatalytic properties. Fig. 3(a–g) depict the absorption spectra of MB dye solution during the photocatalyst process at 0, 2, 5, 7, 10, 12, and 15 min, respectively. The highest absorption peak of the MB solution was found at a wavelength of 664 nm [28]. The dye solution showed an increase in degraded dye when irradiation time increased, as shown in Fig. 3(h). The optimal absorbance of the composite materials at 15 min of photocatalyst activity was the lowest, indicating that the dye was degraded the most.

Before the photolysis measurement, the adsorption of MB solution under dark conditions was tested, as shown in Figs. S6 and S7. The MB solution was not significantly degraded, confirming that the photocatalyst results were due to the properties of the prepared photocatalyst materials. Fig. 4(a). depicts the photocatalytic degradation characteristics of the dye solution as a function of the C/C_0 ratio versus exposure times of light source irritation. Here, C_0 and C were the dye concentrations in the initial aqueous solution (8.75×10^{-6} M) and in the solution after an irradiation time of photocatalytic reaction, respectively. The degradation efficiency [29] was calculated using Eq. (1):

$$\text{Degradation efficiency} = \frac{C_0 - C}{C_0} \times 100. \qquad (1)$$

The degradation efficiencies of CaO/g-C_3N_4 composites with various ratios by weight of CaO:g-C_3N_4: 100%:0, 90%:10%, 80%:20%, 50%:50%, 20%:80%, 10%:90%, and 0:100% were 76.12%, 86.19%, 91.79%, 76.86%, 81.34%, 95.89%, and 71.67%, respectively. The maximum degradation efficiency for 15 min irradiation time was 95.89% with composite material ratio of 10% wt. CaO:90% wt. g-C_3N_4.

The optimized composition values of CaO and g-C_3N_4 were shown in Fig. S8. Comparing the dye decomposition behaviors of pristine CaO, g-C_3N_4, and the composite material ratio of 10% CaO:90% g-C_3N_4 showed that the efficiency of the composite material was higher than both pristine CaO and g-C_3N_4 at the same duration time. Results suggested that the photocatalytic composite materials enhanced the degradation of MB dye. Many works have reported the kinetics of photocatalytic degradation of organic dyes under visible light, as discussed later.

The fixed dye degradation rate was analyzed using Eq. (2) [28].

$$\ln\left(\frac{C}{C_0}\right) = Kt \tag{2}$$

where C_0 and C are the initial concentration of the dye solution (mg/l) and the solution concentration after photocatalytic testing, respectively; K is the reaction rate constant of photocatalytic testing; and t is the irradiation time (min).

The absorbance of the material is shown in Fig. 3, with the dye degradation rate calculated by Eq. (2). The absorbance of the substance, the distance that light passes through the sample or cell width (cm), and the dye concentration (M) followed the Beer-Lambert theory. The dye degradation rate over time was shown in the inset of Fig. 4(a), with the dye degradation rate from the photocatalytic absorbance calculated by Eq. (2). The calculated degradation rate values were 0.0762, 0.1029, 0,1302, 0.0789, 0.0922, 0.1727, and 0.0786 min^{-1} for compositions by weight of 100%:0, 90%:10%, 80%:20%, 50%:50%, 20%:80%, 10%:90%, and 0:100% of CaO:g-C_3N_4, respectively. The highest dye degradation rate was observed at composite material ratio of 10% CaO:90% g-C_3N_4, as 0.1727 min^{-1}, and this ratio was used to test the reusability of the composite. The same composite was used to repeatedly decompose the dye for five cycles, and the results were shown in Fig. 4b. The photocatalytic degradation rates were similar in all five cycles, and the dye was almost completely degraded after 15 min. Therefore, the synthesized composite materials are biodegradable and can also be reused.

Fig. 5 shows the FTIR spectra of the prepared 10% wt. CaO:90% wt. g-C_3N_4 composite sample before and after the photocatalytic process. The spectrum of CaO demonstrated peaks at wavenumbers 2947, 1719, 1145, and 752 cm^{-1} that were identified as the functional groups of O—H, C—O, C—O, and C—O, respectively. The spectrum mixed with g-C_3N_4, showed firm peaks at wavenumbers 3321–3074, 1627, 1400, 1316, 1232, and 809 cm^{-1}, identified as N—H, O—H, C=N, and C—N functional groups, and triazine units of the g-C_3N_4 structure. The small spectral peak of CaO indicated the ratio of the composite materials. More substantial peaks were observed before photocatalysis than after the process. The peaks became clear, and peaks at wavenumbers 2986 and 2905 cm^{-1} were assigned to the O—H group [25, 26]. The change in the O—H peak suggested that the photocatalyst impacted the redox reaction, resulting in the strengthening of the O—H peak, depending on the ability of the CaO/g-C_3N_4 composite, described later as degradation of dyes by photocatalysis.

The photocatalytic mechanism can be used to explain the photocatalytic activity of the composited CaO:g-C_3N_4 material. The optimized composite was observed at 10% wt. g-C_3N_4 with 90% wt. of CaO. The g-C_3N_4 exhibited high attraction due to a high medium band gap (2.70 eV) and good physical properties such as high chemical and thermal stabilities [30]. The medium band gap of g-C_3N_4 composited easily with metal oxides like CaO and quickly motivated the reduction process [31].The excited electron carriers were transferred from the valence band (VB) to the conduction band (CB) to make electron-hole separation. This process occurred more easily when the materials were composited at 10% CaO, with moving charge carrier improvement in the photocatalytic process by the heterojunction structure. This explains why the chemical reaction efficiency of composite materials was greater than the individual materials [30, 31]. Two possible mechanisms for the photocatalytic behavior of CaO/g-C_3N_4 composites were proposed as two scenarios, as shown in Fig. 6. The potential values of the VB and CB of g-C_3N_4 were +1.49 eV/NHE, and −1.15 eV/NHE [32]. The potential values of CaO were performed and calculated as +0.33 eV/NHE and −2.97 eV/NHE for VB and CB levels, respectively [33]. Fig. 6(a) depicts scenario I as the possible mechanism of type-II photocatalyst. In the CB region, the potential of CaO is more negative than g-C_3N_4; thus, the electron carriers are transferred to the CB region of g-C_3N_4 because the negative CB potential of g-C_3N_4 (−1.15 eV/NHE) is more than the standard oxidation-reduction negative potential of $O_2/\cdot O_2^-$ (−0.33 eV/NHE). Therefore, the photogenerated electron carriers on the CB of g-C_3N_4 interact with oxygen to produce superoxide radicals ($\cdot O_2^-$), which initiate the photodegradation process of MB. Furthermore, the VB of both g-C_3N_4 (+1.49 eV/NHE) and CaO (+0.33 eV/NHE) are lower than the standard potential levels of OH/H_2O (+1.99 eV/NHE) and OH/OH^- (+2.40 eV/NHE) [34]. Consequently, the photogenerated holes on VB cannot react with H_2O or OH^-. However, the holes on the VB level of g-C_3N_4 do not exhibit a significant role in the photocatalyst process, with the key role played by $\cdot O_2^-$ radicals. In the degradation reaction, the photogenerated holes stay inactive during the initial process due to the cationic nature of the reactant. [35] The mechanisms are presented in Eqs. (3) to (6) as follows [36, 37].

$$\text{Photocatalyst} + h\nu \longrightarrow \text{Photocatalyst}(e^-_{CB} + h^+_{VB}) \tag{3}$$

$$O_2 + e^- \longrightarrow \cdot O_2^- \quad (4)$$

$$\cdot O_2^- + 2H^+ \longrightarrow 2 \cdot OH \quad (5)$$

$$\cdot OH / \cdot O_2^- + \text{Dye} \longrightarrow \text{Dye degradation} \quad (6)$$

Fig. 6(b) shows scenario II as the other possible mechanism of the z-scheme photocatalyst [36, 37]. This mechanism is similar to the type-II photocatalyst in scenario I, but the electron carriers at the CB of g-C_3N_4 recombine with hole carriers of the VB of CaO; while the photogenerated electron carriers on the CB of CaO interact with oxygen to produce superoxide radicals ($\cdot O_2^-$), which initiate the photodegradation process of MB. The advantage of the z-scheme photocatalyst is that it increases the harvesting of excited light and has a strong redox ability. Therefore, the photocatalytic performance is enhanced.

Table 1 shows comparison of photocatalyst materials on various aspects: synthesis methods, light sources, dye solutions, dye degradation efficiency, and irradiation times. The prepared 10% CaO:90% g-C_3N_4 composite exhibited the optimal dye decomposition properties, a potential candidate for use as a photocatalyst material.

CONCLUSION

CaO/g-C_3N_4 composite materials were successfully prepared from synthesized Cao and g-C_3N_4 particles The physical properties of the composite materials were determined, and the results indicated separation of the mixing phase of CaO and g-C_3N_4. The photocatalytic behaviors of the prepared composites were investigated in an MB aqueous solution under irradiation from a 220 W white light-emitting diode lamp. Results showed that the optimal ratio for dye degradation of the composite materials was 10% CaO:90% g-C_3N_4, giving 95.89% degradation efficiency under 15 min of exposure time at a degradation rate of 0.1727 min^{-1}. The prepared CaO/g-C_3N_4 composite is biodegradable and can be used for five cycles of dye degradation.

Appendix A. Supplementary data

Supplementary data associated with this article can be found at http://dx.doi.org/10.2306/scienceasia1513-1874.2024.066.

Acknowledgements: This work was financially supported by King Mongkut's Institute of Technology Ladkrabang (KMITL) Research Fund, Grant Number: KREF016421. The authors acknowledged the facilities and technical assistance from Nanotechnology and Materials Analytical Instrument Service Unit (NMIS) of College of Materials Innovation and Technology, KMITL.

REFERENCES

1. Gionco C, Paganini MC, Giamello E, Sacco O, Vaiano V, Sannino D (2017) Rare earth oxides in zirconium dioxide: How to turn a wide band gap metal oxide into a visible light active photocatalyst. *J Energy Chem* **26**, 270–276.
2. Desipio MM, Thorpe R, Saha D (2018) Photocatalytic decomposition of paraquat under visible light by carbon nitride and hydrogen peroxide. *Optik* **172**, 1047–1056.
3. Zhou C, Lai C, Zhang C, Zeng G, Huang D, Cheng M, Hu L, Xiong W, et al (2018) Semiconductor/boron nitride composites: synthesis, properties, and photocatalysis applications. *Appl Catal B* **238**, 6–18.
4. Li T, Zhao L, He Y, Cai J, Luo M, Lin J (2013) Synthesis of g-C_3N_4/$SmVO_4$ composite photocatalyst with improved visible light photocatalytic activities in RhB degradation. *Appl Catal B* **129**, 255–263.
5. Al-Madanat O, AlSalka Y, Ramadan W, Bahnemann DW (2021) TiO_2 photocatalysis for the transformation of aromatic water pollutants into fuels. *Catalysts* **11**, 317.
6. Que M, Cai W, Chen J, Zhu L, Yang Y (2021) Recent advances in g-C_3N_4 composites within four types of heterojunctions for photocatalytic CO_2 reduction. *Nanoscale* **13**, 6692–6712.
7. Niju S, Meera KM, Begum S, Anantharaman N (2014) Modification of egg shell and its application in biodiesel production. *J Saudi Chem Soc* **18**, 702–706.
8. Yang L, Huang J, Shi L, Cao L, Yu Q, Jie Y, Fei J, Ouyang H, et al (2017) A surface modification resultant thermally oxidized porous g-C_3N_4 with enhanced photocatalytic hydrogen production. *Appl Catal B* **204**, 335–345.
9. Li X, Zhang J, Shen L, Ma Y, Lei W, Cui Q, Zou G (2009) Preparation and characterization of graphitic carbon nitride through pyrolysis of melamine. *Appl Phys A Mater Sci Process* **94**, 387–392.
10. Dante RC, Martín-Ramos P, Correa-Guimaraes A, Martín-Gil J (2011) Synthesis of graphitic carbon nitride by reaction of melamine and uric acid. *Mater Chem Phys* **130**, 1094–1102.
11. Kumar A, Kumar P, Joshi C, Manchanda M, Boukherroub R, Jain SL (2016) Nickel decorated on phosphorous-doped carbon nitride as an efficient photocatalyst for reduction of nitrobenzenes. *Nanomaterials* **6**, 59.
12. Aljuaid A, Almehmadi M, Alsaiari AA, Allahyani M, Abdulaziz O, Alsharif A, Alsaiari JA, Saih M, et al (2023) g-C_3N_4 based photocatalyst for the efficient photodegradation of toxic methyl orange dye: Recent modifications and future perspectives. *Molecules* **28**, 3199.
13. Bai N, Yin J, Huo X, Ma Y, Guo D, Wang A (2022) *In-situ* synthesis of sodium doped g-C_3N_4 by high temperature copolymerization and photocatalytic performance. *ScienceAsia* **48**, 202–208.
14. Bai N, Qi Y, Miu X, Yin J, Guo D, Wang J, Wang A (2023) Direct blending-drying method of graphitic carbon nitride (g-C_3N_4) with copper chloride solution for enhancement of photocatalytic decolorization of methylene blue. *ScienceAsia* **49**, 192–199.
15. Ismael M (2020) A review on graphitic carbon nitride (g-C_3N_4) based nanocomposites: synthesis, categories, and their application in photocatalysis. *J Alloys Compd* **846**, 156446.
16. Nemiwal M, Zhang TC, Kumar D (2021) Recent progress in g-C_3N_4, TiO_2 and ZnO based photocatalysts for dye degradation: Strategies to improve photocatalytic activity. *Sci Total Environ* **767**, 144896.
17. Ge L, Han C, Liu J (2011) Novel visible light-induced g-C_3N_4/Bi_2WO_6 composite photocatalysts for efficient degradation of methyl orange. *Appl Catal B* **108**,

100–107.
18. Alsohaimi IH, Nassar AM, Elnasr TAS, Cheba BA (2020) A novel composite silver nanoparticles loaded calcium oxide stemming from egg shell recycling: a potent photocatalytic and antibacterial activities. *J Cleaner Prod* **248**, 119274.
19. Singh JP, Lim WC, Won SO, Song J, Chae KH (2018) Synthesis and characterization of some alkaline-earth-oxide nanoparticles. *J Korean Phys Soc* **72**, 890–899.
20. Roy A, Gauri SS, Bhattacharya M, Bhattacharya J (2013) Antimicrobial activity of CaO nanoparticles. *J Biomed Nanotechnol* **9**, 1570–1578.
21. Habte L, Shiferaw N, Mulatu D, Thenepalli T, Chilakala R, Ahn JW (2019) Synthesis of nano-calcium oxide from waste eggshell by sol-gel method. *Sustainability* **11**, 3196.
22. Sánchez-Cantú M, Peralta MDLR, Galindo-Rodríguez AB, Puente-López E, Rubio-Rosas E, Gómez CM, Tzompantzi F (2017) Calcium-containing materials as alternative catalysts in advanced oxidation process. *Fuel* **198**, 76–81.
23. Wen J, Xie J, Chen X, Li X (2017) A review on g-C_3N_4-based photocatalysts. *Appl Surf Sci* **391**, 72–123.
24. Jiang H, Li Y, Wang D, Hong X, Liang B (2020) Recent advances in heteroatom doped graphitic carbon nitride (g-C_3N_4) and g-C_3N_4/metal oxide composite photocatalysts. *Curr Org Chem* **24**, 673–693.
25. Pareek S, Sharma M, Lal S, Quamara JK (2018) Polymeric graphitic carbon nitride-barium titanate nanocomposites with different content ratios: a comparative investigation on dielectric and optical properties. *J Mater Sci Mater Electron* **29**, 13043–13051.
26. Raizada P, Shandilya P, Singh P, Thakur P (2017) Solar light-facilitated oxytetracycline removal from the aqueous phase utilizing a H_2O_2/$ZnWO_4$/CaO catalytic system. *J Taibah Univ Sci* **11**, 689–699.
27. Narkbuakaew T, Sujaridworakun P (2020) Synthesis of tri-S-triazine based g-C_3N_4 photocatalyst for cationic rhodamine B degradation under visible light. *Top Catal* **63**, 1086–1096.
28. Khatua L, Panda R, Nayak AK, Singh A, Sahoo PK, Pradhan D, Singh UP, Das SK (2018) Efficient UV photocatalytic dye decomposition activity with cost effective solid state reaction grown Zinc Orthotitanate (Zn_2TiO_4) nanoparticles. *J Alloys Compd* **764**, 895–900.
29. Barka N, Qourzal S, Assabbane A, Nounah A, Ait-Ichou Y (2008) Factors influencing the photocatalytic degradation of Rhodamine B by TiO_2-coated non-woven paper. *J Photochem Photobiol A* **195**, 346–351.
30. Dong G, Zhang Y, Pan Q, Qiu J (2014) A fantastic graphitic carbon nitride (g-C_3N_4) material: electronic structure, photocatalytic and photoelectronic properties. *J Photochem Photobiol C* **20**, 33–50.
31. Lu X, Wang Q, Cui D (2010) Preparation and photocatalytic properties of g-C_3N_4/TiO_2 hybrid composite. *J Mater Sci Technol* **26**, 925–930.
32. Huo H, Li Y, Wang S, Tan S, Li X, Yi S, Gao L (2022) Construction of highly active $Zn_3In_2S_6$ (110)/g-C_3N_4 system by low temperature solvothermal for efficient degradation of tetracycline under visible light. *Int J Mol Sci* **23**, 13221.
33. Coleto U, Amoresi RAC, Pereira CAM, Schmidt BW, Iani IM, Simões AZ, Monteiro ES, Longo E, et al (2020) Correlation of photocatalytic activity and defects generated in Ca^{2+}-based heterojunctions. *SN Appl Sci* **2**, 1849.
34. Liu R, Yang W, He G, Zheng W, Li M, Tao W, Tian M (2020) Ag-modified g-C_3N_4 prepared by a one-step calcination method for enhanced catalytic efficiency and stability. *ACS Omega* **5**, 19615–19624.
35. Sree GV, Nagaraaj P, Kalanidhi K, Aswathy CA, Rajasekaran P (2020) Calcium oxide a sustainable photocatalyst derived from eggshell for efficient photodegradation of organic pollutants. *J Clean Prod* **270**, 122294.
36. Xu Q, Zhang L, Yu J, Wageh S, Al-Ghamdi AA, Jaroniec M (2018) Direct Z-scheme photocatalysts: Principles, synthesis, and applications. *Mater Today* **21**, 1042–1063.
37. Liao G, Li C, Li X, Fang B (2021) Emerging polymeric carbon nitride Z-scheme systems for photocatalysis. *Cell Rep Phys Sci* **2**, 100355.
38. Xi Q, Gao G, Jin M, Zhang Y, Zhou H, Wu C, Zhao Y, Wang L, et al (2019) Design of graphitic carbon nitride supported Ag-Cu_2O composites with hierarchical structures for enhanced photocatalytic properties. *Appl Surf Sci* **471**, 714–725.
39. Li X, Wan T, Qiu J, Wei H, Qin F, Wang Y, Liao Y, Huang Z, et al (2017) *In-situ* photocalorimetry-fluorescence spectroscopy studies of RhB photocatalysis over Z-scheme g-C_3N_4@Ag@ceAg3PO4 nanocomposites: A pseudo-zero-order rather than a first-order process. *Appl Catal B* **217**, 591–602.
40. Ahmed KE, Kuo DH, Zeleke MA, Zelekew OA, Abay AK (2019) Synthesis of Sn-WO_3/g-C_3N_4 composites with surface activated oxygen for visible light degradation of dyes. *J Photochem Photobiol A* **369**, 133–141.
41. Liu X, Jin A, Jia Y, Xia T, Deng C, Zhu M, Chen C, Chen X (2017) Synergy of adsorption and visible-light photocatalytic degradation of methylene blue by a bifunctional Z-scheme heterojunction of WO_3/g-C_3N_4. *Appl Surf Sci* **405**, 359–371.
42. Alias NH, Jaafar J, Samitsu S, Ismail AF, Mohamed MA, Othman MHD, Rahman MA, Othman NH, et al (2020) Mechanistic insight of the formation of visible-light responsive nanosheet graphitic carbon nitride embedded polyacrylonitrile nanofibres for wastewater treatment. *J Water Proc Eng* **33**, 101015.

Appendix A. Supplementary data

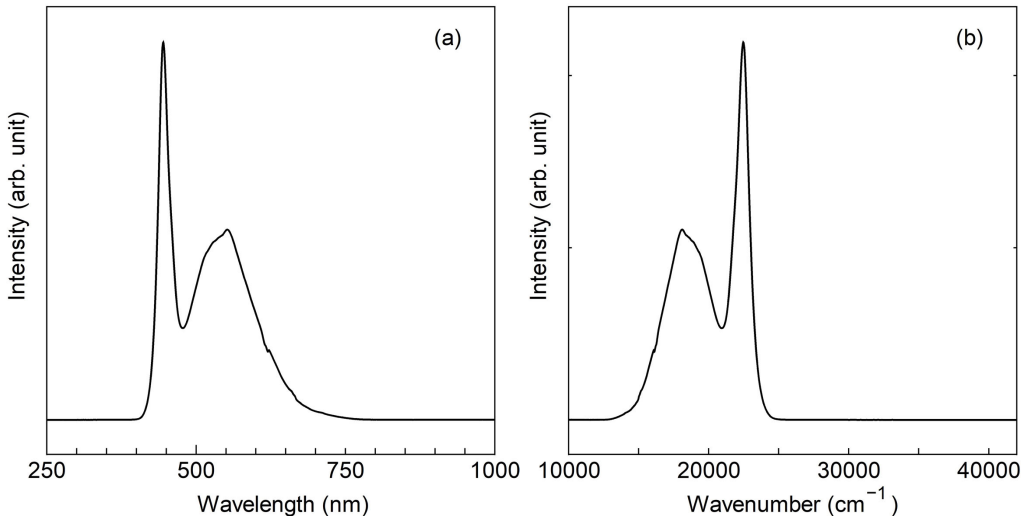

Fig. S1 Optical spectra of an excited 200 W white LED lamp for photocatalyst process plotted against: (a), wavelength and (b), wavenumber.

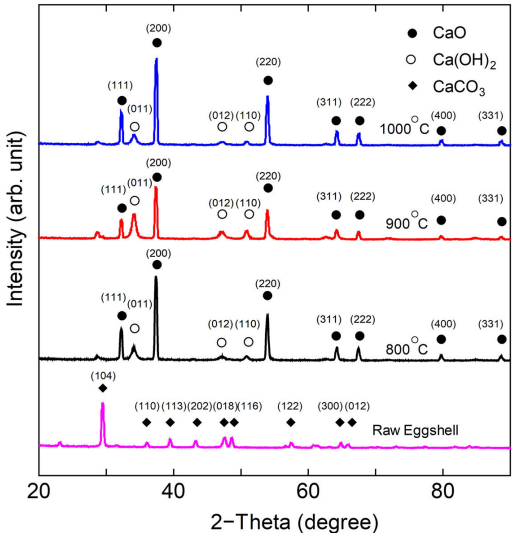

Fig. S2 XRD spectra of CaO derived from eggshells at various calcination temperatures and CaO of raw eggshell.

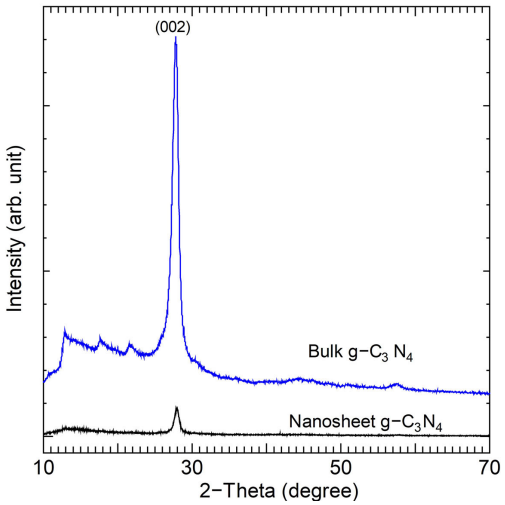

Fig. S3 XRD spectra of thermal synthesized g-C_3N_4 particles.

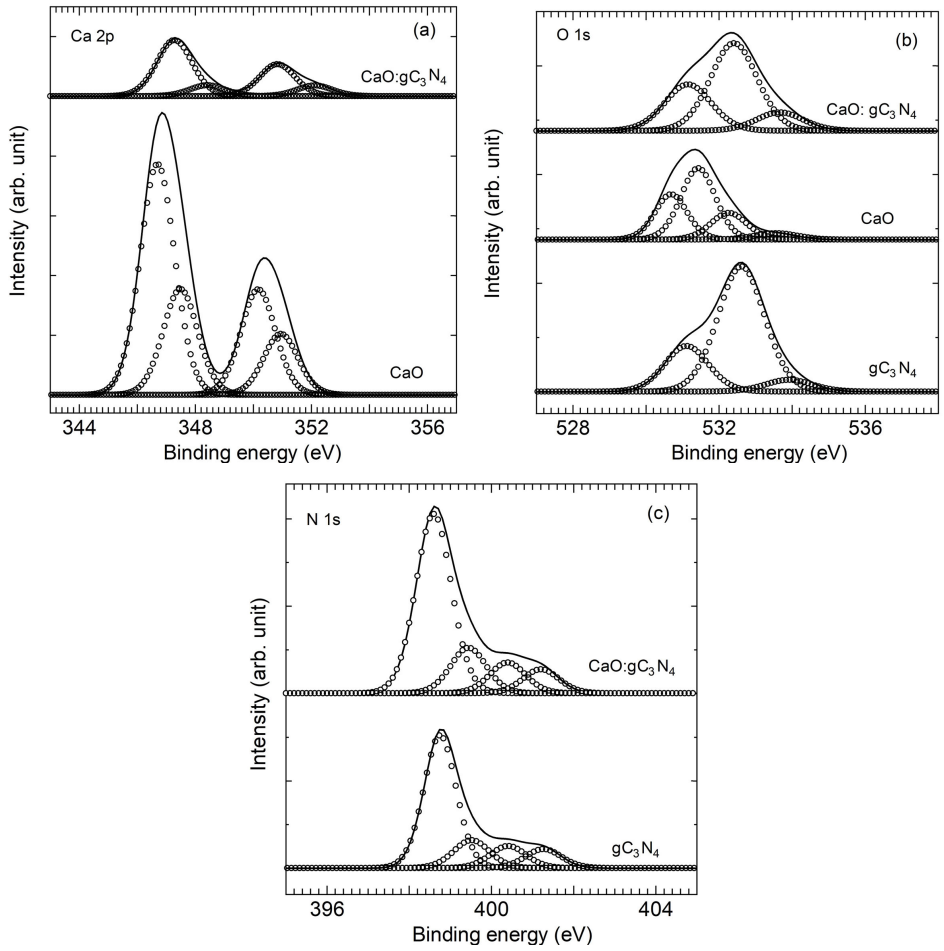

Fig. S4 XPS spectra of: (a), Ca 2p; (b), O 1s; and (c), N 1s.

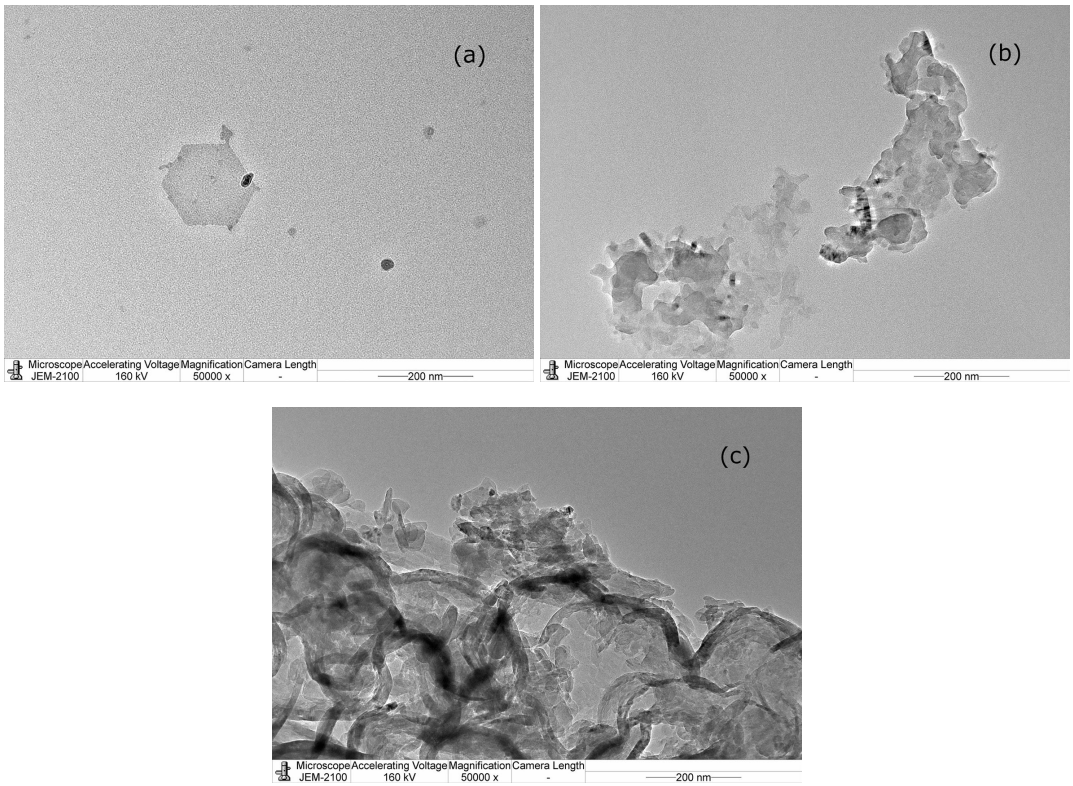

Fig. S5 TEM images of: (a), CaO particles; (b), g-C_3N_4 nanosheet; and (c), Cao/g-C_3N_4 composite of 10% wt. CaO:90% wt. g-C_3N_4.

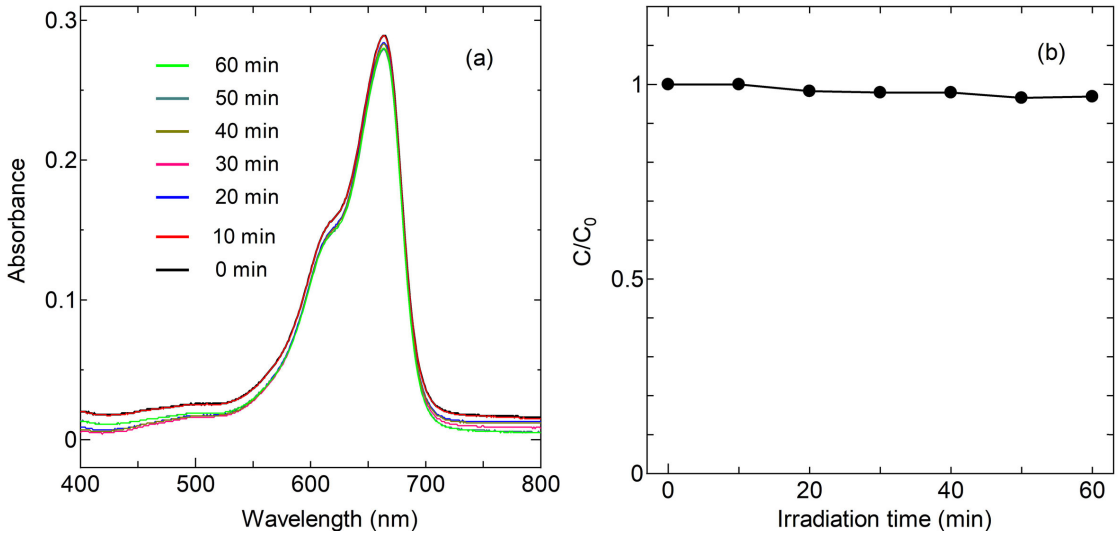

Fig. S6 Photolysis of MB solution without catalyst materials and the C/C_0 values at various irradiation times.

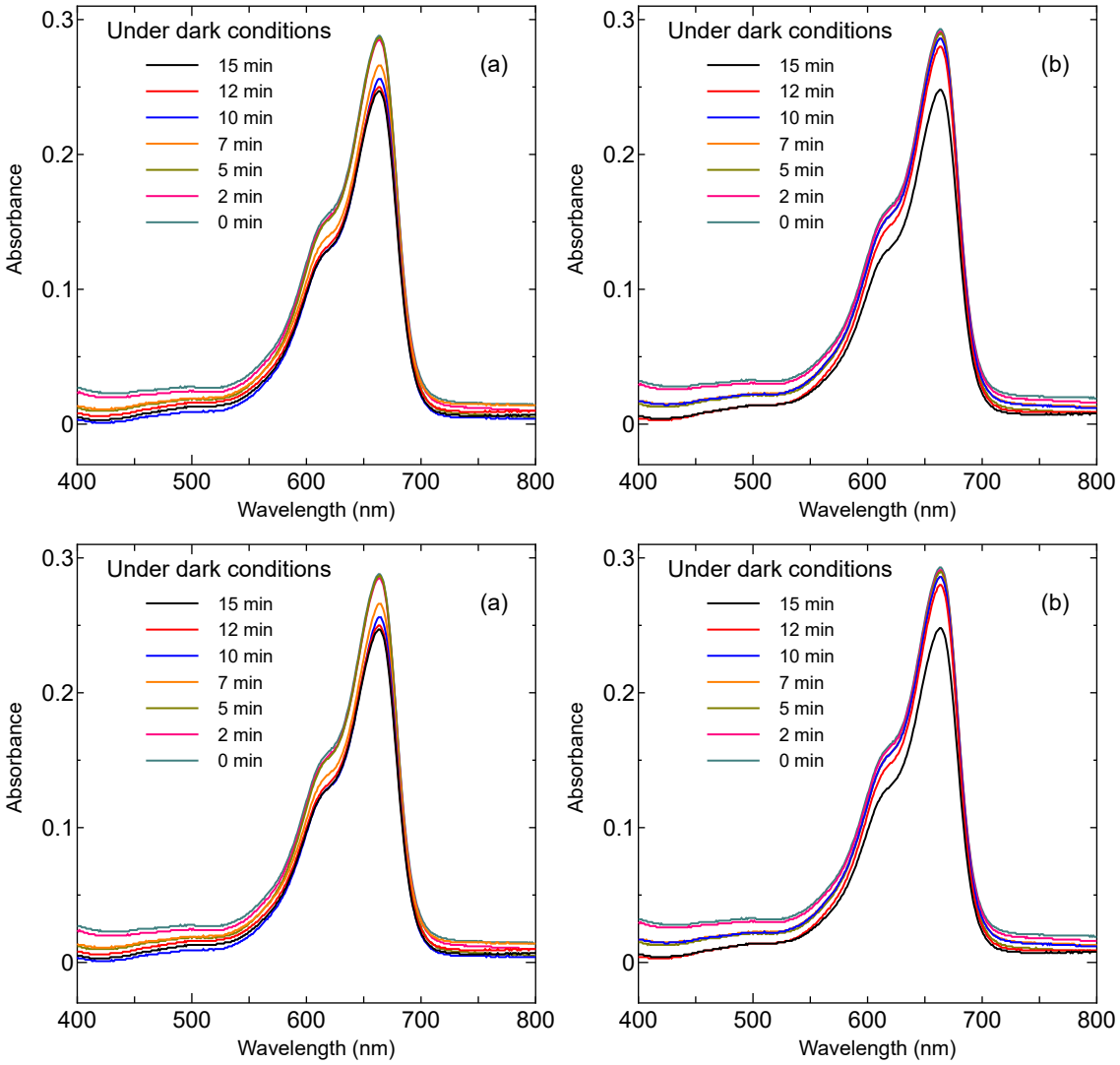

Fig. S7 Comparative photocatalytic activity of: (a), CaO; (b), g-C_3N_4; (c), 10% wt. CaO:90% wt. g-C_3N_4 in MB solution at various times; and (d), the C/C_0 values at different times under dark conditions.

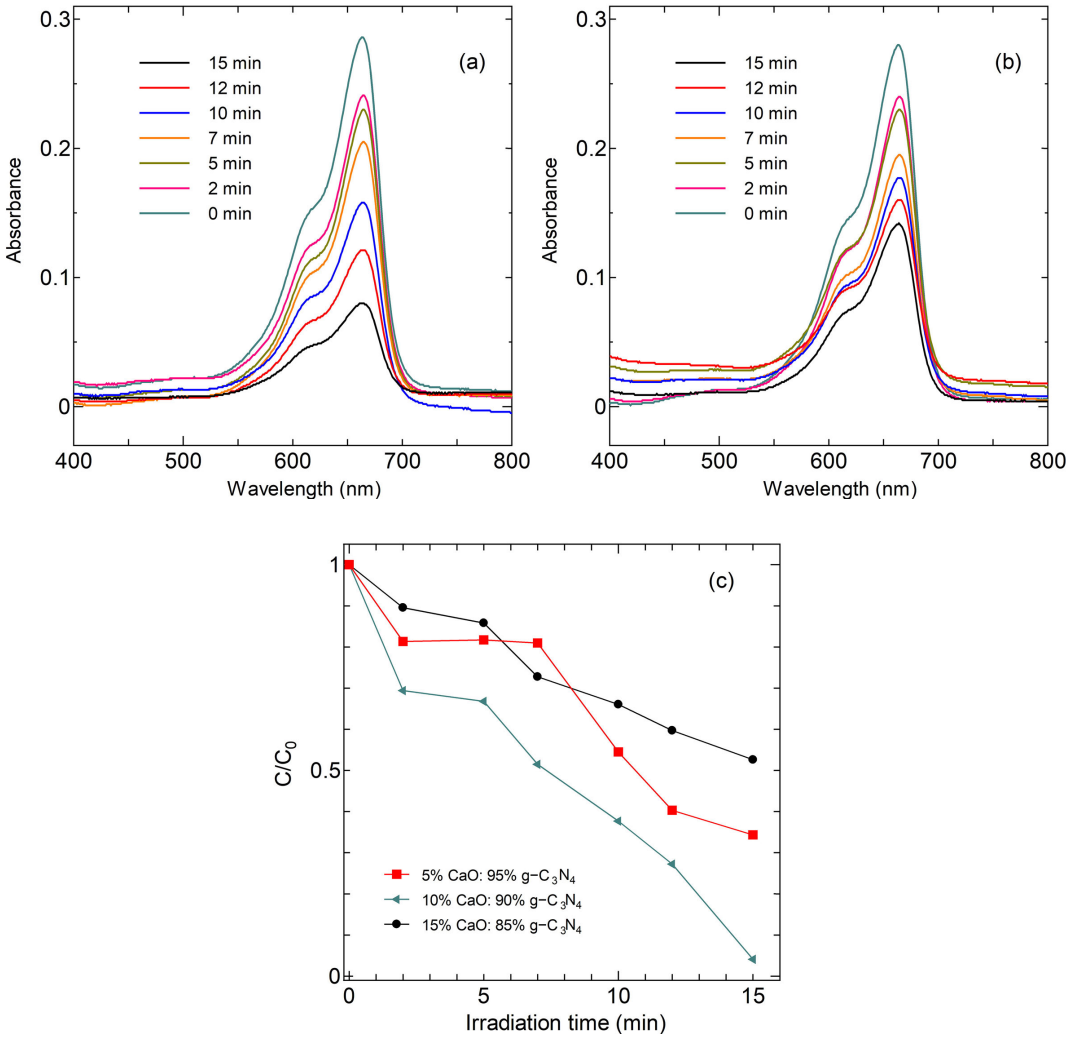

Fig. S8 Comparison of photocatalytic activities of CaO/g-C_3N_4 composites prepared from different ratios (% wt.) of CaO:g-C_3N_4: (a), 5% CaO:95% g-C_3N_4; (b), 15% CaO:85% g-C_3N_4; and (c), the C/C_0 values at different ratios of CaO:g-C_3N_4.